Numerical Simulations of Homogeneous Turbulence using Lagrangian-Averaged Navier-Stokes Equations

By Kamran Mohseni †, Steve Shkoller ‡, Branko Kosović ‡, Jerrold E. Marsden †, Daniele Carati ¶, Alan Wray ‖, and Robert Rogallo ‖

The Lagrangian-averaged Navier-Stokes equations (LANS) are numerically evaluated as a turbulence closure. They are derived from a novel Lagrangian averaging procedure on the space of all volume-preserving maps and can be viewed as a numerical algorithm which removes the energy content from the small scales (smaller than some *a priori* fixed spatial scale α) using a dispersive rather than dissipative mechanism, thus maintaining the crucial features of the large scale flow. We examine the modeling capabilities of the LANS equations for decaying homogeneous turbulence, ascertain their ability to track the energy spectrum of fully resolved direct numerical simulations (DNS), compare the relative energy decay rates, and compare LANS with well-accepted LES models.

1. Introduction

Over the last thirty years direct numerical simulation of turbulent flows at small to moderate Reynolds numbers has been a valuable asset in understanding turbulence phenomena. In such simulations the motion of eddies ranging in size down to the Kolmogorov dissipation length scale are explicitly accounted for. The main difficulty in the turbulence engineering community is that performing the DNS of typical engineering problems (usually at high Reynolds numbers) is very expensive, and therefore unlikely to happen in the foreseeable future. This is mainly because the number of degrees of freedom for three-dimensional Navier-Stokes flow grows rapidly with Reynolds number; namely it is proportional to $\mathrm{Re}^{9/4}$. Consequently, increasing the Reynolds number by a factor of 2 will increase the memory size by a factor of 5 and the computational time by a factor of 10.

There are methods for simulating turbulent flows where one does not need to use the brute-force approach in DNS of resolving all scales of motion. A popular alternative is Large Eddy Simulation (LES) in which only large scales of motion are resolved while the effect of small scales is modeled. The basic idea behind LES is to define a large scale field through a low-pass filtering of the flow variables; therefore, the governing equations for the mean flow quantities (large scales) are obtained by filtering the Navier-Stokes and continuity equations. In inhomogeneous, *e.g.*, wall bounded, flows, the filter width must be a function of position so as to capture the average size of the turbulent eddies that vary in space.

† Division of Engineering and Applied Science, California Institute of Technology.
‡ Department of Mathematics, University of California, Davis.
¶ Unite de Physique Stat. et des Plasmas, Universite Libre de Bruxelles, Brussels, Belgium.
‖ Center for Turbulence Research, NASA Ames.

Another method is the Reynolds averaging of the Navier-Stokes equations, or RANS. In this approach the flow field is decomposed into a time- or ensemble- averaged mean flow and a fluctuating perturbation field. Substitution of this field decomposition into the Navier-Stokes equations results in a set of differential equations for the mean flow quantities containing contributions from the time-varying, turbulent motion. This requires the introduction of a turbulence model to describe the effect of these fluctuations on the mean.

The closure problem in LES is a central issue in turbulence modeling. It is believed that turbulence at small scales retains a higher level of homogeneity, which makes it more susceptible to modeling. The rationale is that only the large-scale motions are noticeably affected by the geometry of the domain, while the small scale motions are self-similar or even universal throughout the bulk of the flow. Hence, the main goal of LES modeling is to accurately model the net effect of small scales (subgrid scales) on the dynamics of large scales (grid scales) without solving for the evolution of small scales.

In this study, we consider a new approach introduced in Marsden & Shkoller (2000). Unlike the traditional averaging or filtering approach used for both RANS and LES, wherein the Navier-Stokes equations are averaged, the novel Lagrangian approach is based on averaging at the level of the variational principle from which the Navier-Stokes equations are derived. Namely, a new averaged action principle is defined. The least action principle then yields the so-called Lagrangian-averaged Euler (LAE) equations when the flow is deterministic; when the flow is a stochastic process and covariant derivatives are replaced by mean backward-in-time stochastic derivatives, the Lagrangian-averaged Navier-Stokes equations (LANS) are obtained, via the Ito formula of stochastic calculus (just as the Navier-Stokes equations are obtained from the usual non-averaged action principle).

The averaged Euler models were introduced on all of $\mathbb{R}^3$ (the three-dimensional Euclidean space) in Holm *et al.*(1998), on boundaryless manifolds in Shkoller (1998), on bounded subsets of $\mathbb{R}^3$ with boundary in Marsden, Ratiu, & Shkoller (2000), and on manifolds with boundary in Shkoller (2000a); they were derived to model the mean motion of incompressible flows. A short review of the derivation of the Lagrangian-averaged equations is presented in Section 2.

In this study, we shall concentrate on homogeneous flows, specifically on decaying isotropic turbulence. Such flows are unbounded and thus differ from flow in regions near solid boundaries, but they provide an ideal test case for the adjustment and verification of new turbulence theories and models. An anisotropic version of the LANS equations was recently developed by Marsden & Shkoller (2000). The modeling capabilities of the anisotropic LANS in channel flows will be the topic of a future publication. The anisotropic model provides a natural "dynamic" rescaling that allows the spatial scale for the averaging ($\alpha^2 F$ defined in the next section) to be time dependent as well as orientation dependent.

This report is organized as follows. In the next section a review of the LANS equations is presented. The numerical technique adopted in this study is described in Section 3. Our main numerical results are presented in Section 4 where computations on LAE as well as LANS equations are discussed. Some strategies for calculating the initial Lagrangian-averaged velocity field from the DNS data are discussed. Our findings are summarized in Section 5.

2. Lagrangian-Averaged Navier-Stokes Equations

In this section, we give a brief summary of the relevant background material on the Lagrangian averaging approach and the resulting Lagrangian averaged Euler (LAE) and Lagrangian-averaged Navier-Stokes (LANS) equations. The detailed derivation of the LAE/LANS equations can be found in the article Marsden & Shkoller (2000). Analytic results for classical solutions to these equations can be found in Shkoller (1998), Foias *et al.*(1999), Shkoller (2000a), Marsden, Ratiu, & Shkoller (2000), Oliver & Shkoller (2000), and Shkoller (2000b).

2.1. *Lagrangian averaging*

The Reynolds decomposition is an Eulerian decomposition of the spatial velocity field of the fluid. The Lagrangian averaging procedure takes an entirely different starting point, by decomposing instead the Lagrangian flow of the velocity field. Let $\eta(t,x)$ be the volume-preserving Lagrangian flow of the random variable $u(t,x)$ so that η satisfies the ordinary differential equation $\partial_t\eta(t,x) = u(t,\eta(t,x))$ (or its stochastic counterpart) with initial condition $\eta(0,x) = x$. We choose a stochastic process $\xi^\alpha(t,x)$, parameterized by $\alpha > 0$, such that $\xi^{\alpha=0}(t,x) = x$ for all time t, and for all t and $\alpha > 0$, the map $\xi^\alpha(t,\cdot) : \Omega \to \Omega$ is a volume-preserving near-identity diffeomorphism. We denote the stochastic derivative of ξ^α with respect to α at $\alpha = 0$ by ξ'; if the map $t \mapsto \xi^\alpha(t,\cdot)$ were smooth, the vector ξ' would be given simply by $\xi'(t,x) = (d/d\alpha)|_{\alpha=0}\xi^\alpha(t,x)$. The stochastic process ξ' is an element of a probability space $\mathcal{P}$ with measure dP, and by construction has expected value zero, $\overline{\xi'} = 0$, i.e., ξ' has mean zero.

We then define a macroscopic flow field $\eta^\alpha(t,x)$ by

$$\eta^\alpha(t,x) = (\xi^\alpha)^{-1}(t,\eta(t,x))), \tag{2.1}$$

or in shorthand notation

$$\eta^\alpha_t = (\xi^\alpha_t)^{-1} \circ \eta_t.$$

η^α is the *fuzzy* particle placement field which is only accurate down to the spatial scale α; namely, a particle labeled x in the fluid container at $t = 0$ is mapped by $\eta^\alpha(t,\cdot)$ to its new position at time t, and this new position $\eta^\alpha(t,x)$ can be determined only to within a distance α of the exact position $\eta(t,x)$. The decomposition (2.1) is a nonlinear Lagrangian decomposition of maps on the group of volume-preserving diffeomorphisms. There is no vector-space structure on this group, so it is not appropriate to suppose an additive decomposition as in the Reynolds decomposition.

We next define the corresponding spatial velocity fields u^α and w^α associated, respectively, with the flows η^α and ξ^α. In particular, we define these velocities by

$$\partial_t\xi^\alpha(t,x) = w^\alpha(t,\xi^\alpha(t,x)), \quad \partial_t\eta^\alpha(t,x) = u^\alpha(t,\eta^\alpha(t,x)).$$

It is now possible, by differentiating (2.1) with respect to time t, to obtain the relationship between u, u^α, and w^α. We find that

$$u^\alpha(t,x) = D(\xi^\alpha)^{-1}(x) \cdot \left[u(t,\xi^\alpha(t,x) - w^\alpha(t,\xi^\alpha(t,x))\right]. \tag{2.2}$$

The notation $D(\xi^\alpha)^{-1}(x)$ means the matrix of partial derivatives of the inverse map $(\xi^\alpha)^{-1}$ evaluated at the point x in Ω.

Now, the inviscid portion of the dynamics of the Navier-Stokes equations is governed by a simple variational principle, or action, which is just the time integral of the kinetic

energy of divergence-free vector fields:

$$S = \frac{1}{2}\int_{t_0}^{t_1}\int_{\Omega} |u(t,x)|^2 dxdt.$$

The Euler-Lagrange equations for $S(u)$ are the incompressible Euler equations, and if one allows the flow of the Euler solution to undergo a random walk, then the Navier-Stokes equations immediately arise (see Chorin (1973) and Peskin (1985)).

In order to obtain Lagrangian-averaged Navier-Stokes equations we shall define an averaged variational principle using our macroscopic or fuzzy Lagrangian description of the fluid. As such, we define the averaged action by

$$S^{\alpha} = \frac{1}{2}\int_{t_0}^{t_1}\int_{\Omega}\int_{\mathcal{P}} |u^{\alpha}(t,x)| dP dxdt, \tag{2.3}$$

where we have averaged over all possible perturbations or Lagrangian fluctuations of the exact flow.

At this stage, we asymptotically expand $u^{\alpha}(t,x)$ about $\alpha = 0$, and make the Taylor hypothesis that the Lagrangian fluctuation is frozen into the mean flow. We obtain (after a convenient rescaling) that

$$u^{\alpha}(t,x) = u(t,x) + 2\alpha \,\mathrm{Def}\, u(t,x)\cdot\xi'(t,x) + O(\alpha^3), \tag{2.4}$$

where

$$\mathrm{Def}\,\mathbf{u} = \frac{1}{2}\left[\nabla\mathbf{u} + (\nabla\mathbf{u})^T\right].$$

Notice that $u(t,x)$ is the mean of u^{α} since $\overline{u^{\alpha}} = u$, and that to $O(\alpha^3)$, $\mathrm{Def}\, u\cdot\xi'$ is the Eulerian fluctuation. Defining the Lagrangian covariance or fluctuation tensor by

$$F(t,x) = \int_{\mathcal{P}} \xi'\otimes\xi' dP, \tag{2.5}$$

substituting the expansion (2.4) into (2.3), and truncating at $O(\alpha^3)$, we obtain the first-order averaged action principle S_1^{α} as a function of the divergence-free mean u and the covariance F:

$$S_1^{\alpha}(u,F) = \frac{1}{2}\int_{t_0}^{t_1}\int_{\Omega}\left[u\cdot u + 2\alpha^2 F : (\mathrm{Def}\, u\cdot \mathrm{Def}\, u)\right] dxdt. \tag{2.6}$$

2.2. *The LANS and LAE equations*

We define the fourth-rank symmetric tensor C by complete symmetrization of $F\otimes \mathrm{Id}$, so that in coordinates

$$C^{ijkl} = \frac{1}{4}\left(F^{lj}\delta^{ik} + F^{kj}\delta^{il} + F^{li}\delta^{jk} + F^{ki}\delta^{jl}\right);$$

we then define the linear operator $\mathcal{C}$, mapping divergence-free vector fields into vector fields, by $\mathcal{C}u = \mathrm{Div}(C : \nabla u)$. By letting the Lagrangian flow of the mean velocity undergo Brownian motions, and computing the first variation of $S_1^{\alpha}(u,F)$, we obtain the anisotropic Lagrangian-averaged Navier-Stokes equations (LANS) for the mean velocity as

$$\partial_t u + (u\cdot\nabla)u + \mathcal{U}^{\alpha}(u,F) = -(1-\alpha^2\mathcal{C})^{-1}\,\mathrm{grad}\, p + \nu\triangle u, \tag{2.7}$$

where

$$\begin{aligned}\mathcal{U}^\alpha(u,F) :=& \alpha^2(1-\alpha^2\mathcal{C})^{-1}\Big\{-\frac{1}{2}\operatorname{Div}\left[\operatorname{Def} u\cdot(\pounds_u F)+(\pounds_u F)\cdot\operatorname{Def} u\right]\\ &-\operatorname{Div} C:(\nabla u\cdot\nabla u)-C\vdots\nabla(\nabla u\cdot\nabla u)\\ &-C\vdots\operatorname{Div}(\nabla u\otimes\nabla u)+(\operatorname{Div}[\nabla C:\nabla u])\cdot u\\ &-(\nabla u)^T\cdot\mathcal{C}u+2F:\nabla(\operatorname{Def} u^2)-4\operatorname{Div}[F\cdot\operatorname{Def} u^2]\Big\}. \end{aligned}\tag{2.8}$$

The notation $\pounds_u F$ means the Lie derivative of the tensor F in the direction u, and $\cdot$, $:$, etc., means contraction of indices as many times as dots appear. The term $\mathcal{U}^\alpha(u,F)$ is analogous to the term $\operatorname{Div}\overline{u'\otimes u'}$ in the RANS equation which is the divergence of the Reynolds stress. As we noted, the LANS formulation provides a natural turbulent-closure.

In addition to the evolution equation for the mean given by (2.7), the calculus of variations also provides the evolution equation for the covariance tensor as

$$\partial_t F+\pounds_u F=0.\tag{2.9}$$

These two coupled systems of evolution equations are supplemented by the incompressibility constraint $\operatorname{div} u=0$, initial conditions $u(0,x)=u_0(x)$, and boundary conditions, for example no slip, $u=0$ on $\partial\Omega$.

After solving the LANS equations for the mean velocity u, one can then solve for the Eulerian fluctuations $2\alpha\operatorname{Def} u\cdot\xi'$ and "correct" the macroscopic velocity field to $O(\alpha^3)$. This does not require the solution of the Navier-Stokes equations; instead, simple linear advection problems for ξ' need to be solved. Letting the vector ξ' have Cartesian components (ξ_1,ξ_2,ξ_3), these equations are given in component form by

$$\partial_t\xi_i+\xi_i,ju^j+u^j,i\xi_j=0.\tag{2.10}$$

Equation (2.10) is obtained from the Taylor hypothesis (Marsden & Shkoller (2000)) and plays the role of the "corrector" in the theory of homogenization.

Equations (2.7) and (2.9) are *anisotropic*, allowing for fluctuation effects to depend on position and direction. There is a corresponding *isotropic* theory in which it is assumed that the covariance tensor F is everywhere equal to the identity Id. In this case, the first-order averaged action principle $S^\alpha_{1,\mathrm{iso}}$ is only a function of the mean velocity u, and is given by

$$S^\alpha_{1,\mathrm{iso}}(u)=\frac{1}{2}\int_{t_0}^{t_1}\int_\Omega\left[u\cdot u+2\alpha^2\operatorname{Def} u:\operatorname{Def} u)\right]dxdt.\tag{2.11}$$

Applying the calculus of variations machinery to (2.11) yields the isotropic LANS equation

$$\begin{gathered}\partial_t u+(u\cdot\nabla)u+\mathcal{U}^{\alpha,\mathrm{iso}}(u)=-(1-\alpha^2\Delta)^{-1}\operatorname{grad} p+\nu\Delta u,\\ \operatorname{div} u=0,\quad u(0,x)=u_0(x),\\ u=0\text{ on }\partial\Omega,\end{gathered}\tag{2.12}$$

where

$$\mathcal{U}^{\alpha,\mathrm{iso}}(u)=\alpha^2(1-\alpha^2\Delta)^{-1}\operatorname{Div}\left[\nabla u\cdot\nabla u^T+\nabla u\cdot\nabla u-\nabla u^T\cdot\nabla u\right].\tag{2.13}$$

The most obvious scenario in which one might assume the covariance is isotropic is in decaying turbulence inside a periodic box. In this case, the isotropic LANS equations are

given by

$$\begin{aligned} \partial_t u + (u \cdot \nabla)u + \operatorname{Div} \mathcal{S}^\alpha(u) &= -\operatorname{grad} p + \nu \Delta u, \\ \operatorname{div} u &= 0, \end{aligned} \tag{2.14}$$

with periodic boundary conditions imposed. $\mathcal{S}^\alpha(u)$ is the *Lagrangian subgrid stress tensor* defined by

$$\mathcal{S}^\alpha(u) = \alpha^2 (1 - \alpha^2 \Delta)^{-1} \left[\nabla u \cdot \nabla u^T + \nabla u \cdot \nabla u - \nabla u^T \cdot \nabla u \right].$$

Appropriate interpretation of the Lagrangian averaging process of the DNS data is crucial in any successful comparison of the LANS computations with the DNS results. A few different techniques for initializing LANS equations were considered in this study. Apart from the truncation of the DNS data to the resolution of LANS simulations, we have initialized LANS simulations by Helmholtz filtering or spatially averaging of the DNS data. For the numerical simulations on the experiment by Comte-Bellot & Corrsin (1966) and (1971) we found that using the filter based on the Helmholtz operator or spatial averaging (top hat filter) resulted in a severe reduction of the initial resolved kinetic energy to a fraction of that of a field truncated in Fourier space (i.e., using a Fourier cut-off filter). We point out that such a reduction is independent of the model used and diminishes the value of the tests. Consequently, all of the LANS results reported in this study are initialized by sharply truncating the DNS data to the resolution of the LANS calculation.

3. Numerical Method

In this study we focus on the numerical solution of homogeneous turbulence. Our computational domain is a periodic cubic box of side 2π. In a numerical simulation of decaying turbulence, the size of the computational domain puts an upper bound on the growth of the large scales in the flow. This is consistent with the observation in most experiments that the largest scales of motion are of the same order as the size of the experimental apparatus. Given the number of grid points and the size of the computational domain, the smallest resolved length scale or equivalently the largest wave number, k_{max}, is prescribed. In a three-dimensional turbulent flow the kinetic energy cascades in time to smaller, more dissipative scales. The scale at which viscous dissipation becomes dominant, and which represents the smallest scales of turbulence, is characterized by the Kolmogorov length scale η. In a fully resolved DNS, the condition $k_{max}\eta \gtrsim 1$ is necessary for the small scales to be adequately represented. Consequently, k_{max} limits the highest achievable Reynolds number in a direct numerical simulation for a given computational box.

The full range of scales in a turbulent flow for even a modest Reynolds number spans many orders of magnitude, and it is not generally feasible to capture them all in a numerical simulation. On the other hand, in turbulence modeling, empirical or theoretical models are used to account for the net effect of small scales on large energy- containing scales. In the next section, the numerical simulations of decaying homogeneous turbulence based on the full DNS, LES modeling, and LANS modeling are presented.

The core of the numerical method used in this study is based on a standard parallel pseudospectral scheme with periodic boundary conditions similar to the one described in Rogallo (1981). The spatial derivatives are calculated in the Fourier domain, while the nonlinear convective terms are computed in physical space. The flow fields are advanced

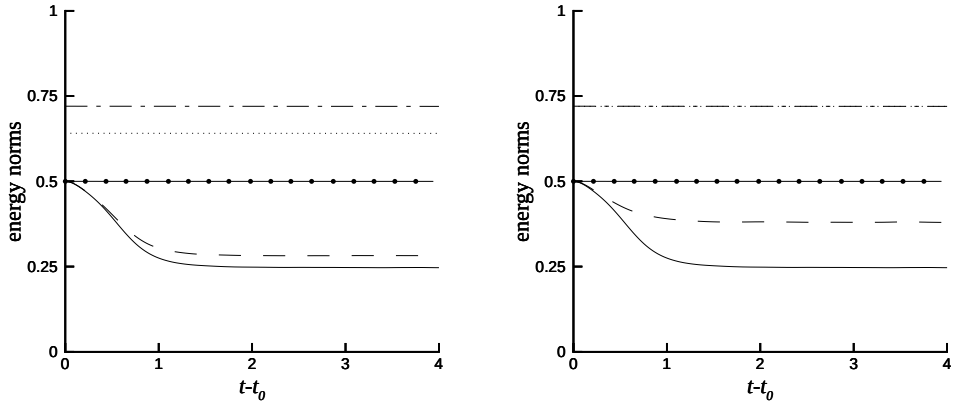

FIGURE 1. LAE simulation $t - t_0 = 1.8$, Euler (solid with circles) (a) $N_\alpha^3 = 64^3$; for $\alpha = \frac{1}{16}$, $E_{L_2}(\mathbf{u})$ (solid), $E_{H^1}(\mathbf{u})$ (dash dot); for $\alpha = \frac{1}{20}$, $E_{L_2}(\mathbf{u})$ (dashed), $E_{H^1}(\mathbf{u})$ (dotted); (b) $\alpha = \frac{1}{16}$; with $N_\alpha^3 = 48^3$; $E_{L_2}(\mathbf{u})$ (solid), $E_{H^1}(\mathbf{u})$ (dash dot); and with 64^3, $E_{L_2}(\mathbf{u})$ (dashed), $E_{H^1}(\mathbf{u})$ (dotted). Note that in case (b) the curves for $E_{H^1}(\mathbf{u})$ for the different resolutions coincides.

in time in physical space using a fourth order Runge-Kutta scheme. The time step was chosen appropriately to ensure numerical stability. To eliminate the aliasing errors in this procedure the two thirds rule is used, so that the upper one third of wave modes is discarded at each stage of the fourth order Runge-Kutta scheme.

In addition to LANS we also performed simulations using a dynamic SGS model (Germano *et al.*(1994). Germano *et al.*(1994) suggested a dynamic procedure in which the model coefficient of an arbitrary functional relationship, selected to represent the subgrid scale stress tensor, can be evaluated as part of the simulation. This procedure, applied to the Smagorinsky eddy-viscosity model, has proven quite versatile and is used here as a representative of a class of LES models. The filter aspect ratio in the dynamic model is a free parameter and the final result depends on the value of this parameter particularly in severe test cases such as the one considered here. In order to avoid introducing any further arbitrary parameters, no averaging operation is performed on the model coefficients over the computational domain. However, the LES computations were repeated for various filter aspect ratios, and the parameter that matched the best with the turbulence decay of the DNS data was used in the computations of the next section.

4. Results

In this section, we present results of our numerical simulations of the LANS equations. We first demonstrate the dispersive characteristic of the energy cascade in the LAE equations.

4.1. *Lagrangian-Averaged Euler Equations*

In section 2, we argued that the LAE equations redistribute the energy content among the small scales through a nonlinear dispersive mechanism. This is illustrated in Figure 1 where various energy norms in the LAE simulations (*i.e.*, no viscous dissipation) are contrasted against the energy norm in the Euler equations. The initial condition is the

same as the one described in the next section for the viscous computations. As expected, the H^1(-equivalent) norm of the energy for the LAE equations, given by

$$E_{H^1}(\mathbf{u}) = \frac{1}{2}\int \left[\mathbf{u}\cdot\mathbf{u} + 2\alpha^2\,\mathrm{Def}\,\mathbf{u}\cdot\mathrm{Def}\,\mathbf{u}\right]\, d^3x, \tag{4.1}$$

is a conserved quantity. In the case of periodic boundary conditions, this energy function may also be expressed as $E_{H^1} = \frac{1}{2}\int \mathbf{u}\cdot(1-\alpha^2\Delta)\mathbf{u}$. The value of E_{H^1} depends on the initial condition, as well as the parameter α. For given initial data and fixed α, on the other hand, the L_2 energy function

$$E_{L_2}(\mathbf{u}) = \frac{1}{2}\int \mathbf{u}\cdot\mathbf{u}\; d^3x \tag{4.2}$$

drops significantly from its normalized initial value of 0.5. It is precisely the quantity $E_{L_2}(\mathbf{u})$ that we shall compare with the numerical simulation of Navier-Stokes equations. Again, the absolute drop in $E_{L_2}(\mathbf{u})$ depends on the initial velocity as well as the value of α. Since $E_{H^1}(\mathbf{u})$ is constant along solutions of the LAE equations, any decay in $E_{L_2}(\mathbf{u})$ is followed by an increase in $\alpha^2 E_{L_2}(\nabla u)$. After some initial transient all of the energy norms saturate. We remark that, when $\alpha = 0$, the H^1 energy norm (4.1) reduces to the usual L^2 kinetic energy.

In a viscous computation the dispersive decay in $E_{L_2}(\mathbf{u})$ is augmented by the viscous decay in $E_{L_2}(\mathbf{u})$, as the viscous effects remove energy from small scales. Viscous computations are performed in the next section to quantify the nature of the viscous decay.

In figure 1(b) the effect of grid resolution on LAE simulations is shown. While the value of $E_{H^1}(\mathbf{u})$ is the same in both 48^3 and 64^3 runs, the L_2 norm of $\mathbf{u}$ and $\nabla\mathbf{u}$ are significantly different after an initial transient. Therefore the dispersive decay in $E_{L_2}(\mathbf{u})$ strongly depends on the size of the computational domain. However, it is expected that if the smallest resolved scale in the LAE simulations is located in a subinertial range with low energy compared to the peak of the energy spectra, any variation of $E_{L_2}(\mathbf{u})$ with the size of the computational domain would be small. This issue requires further investigation by computations based on an initial field with a large inertial range.

One should note that the conservation of the H^1 norm is slightly sensitive to the accuracy of the implemented numerical scheme. The fourth order Runge-Kutta has proved to be adequate in our case. However, numerical experimentation has shown that lower-order time integration schemes might result in a slight decay in the H^1 norm. All of the reported computations in this study are performed using the same fourth order Runge-Kutta scheme.

4.2. *Decaying turbulence*

The most widely used published data on decaying grid turbulence are due to Comte-Bellot & Corrsin (1966) and (1971) which we will hereafter refer to as CBC. Their data is well documented and has been used widely in the development of DNS, LES, and other turbulence models.

The DNS computations in this study were carried out on the Hewlett-Packard Exemplar V2500 at Caltech. The initial field is taken from Wray (1998). Wray provides a filtered velocity field in physical space, derived from 512^3 data by a sharp truncation in Fourier space to 128^3. All of the computations performed in this study were started with this data. The initial Taylor Reynolds number is $\mathrm{Re}_\lambda = 72$.

The evolution of the energy spectrum as predicted by DNS using 128^3 points is il-

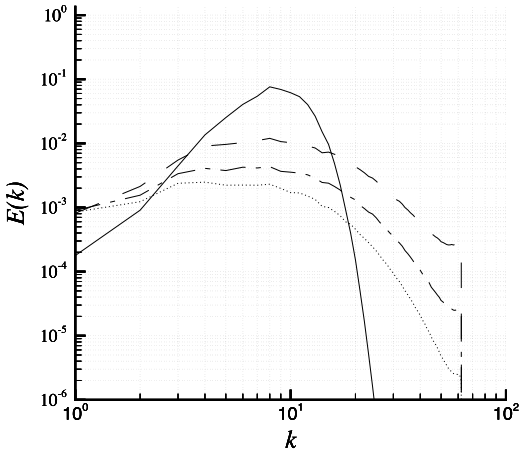

FIGURE 2. Spectrum of the energy, $\mathrm{Re}_\lambda = 72$, $N_{DNS}^3 = 128^3$, $t = 0$ (solid); $t = 1$ (dash); $t = 2$ (dash dot); $t = 3$ (dotted).

lustrated in figure 2. The energy of fully developed isotropic turbulence decays in time while the scales of motion grow; the resulting Re_λ decreases with time. Consequently, a well resolved, fully developed field will remain well resolved as it decays. On the other hand, the integral scales grow in time and will eventually become comparable to the size of the computational box. Since the computational box contains only a small sample of the largest representable eddies, eventually the computation will suffer from a lack of sample in the energy-containing scales. The rather wide initial energy spectrum with a peak around the eighth Fourier mode provides a harsh test case for any turbulence model at such a resolution. As is the case with most subgrid models LANS model is expected to perform better when energy containing range is well resolved. In other words the model is expected to perform better when the spectral energy peaks at a lower wave number. The simulation of CBC experiment at $\mathrm{Re}_\lambda = 72$ used in this study barely satisfy this criterion and provide a severe test case of the LANS turbulence modeling capability. However, this does not imply that the developed inertial rage is required for the model to reach optimal performance.

The best behavior of LANS modeling is expected for applications in which the scale α is within, or at least close to, an inertial subrange. The CBC experiments at $\mathrm{Re}_\lambda = 72$ barely satisfy this criterion and provide a severe test case of the LANS turbulence modeling capability.

The evolution of total kinetic energy (TKE) of the DNS data is contrasted against various dynamic LES and LANS simulations in figure 3, for two resolutions: 48^3 and 64^3. TKE's for DNS data, sharply filtered to the resolution of the LES and LANS computations, are also presented. The best match between the DNS data and the dynamic LES results is achieved for a filter aspect ratio of 2 and 4 in the 48^3 and 64^3 calculations, respectively. In the 64^3 computation both LES and LANS satisfactorily predict the decay rate. However, at the lower resolution of 48^3 both models underestimate the decay rate, with the LANS model being more under-dissipative. It is clear that at such a low resolution the energy-containing part of the spectrum is barely resolved. This is demonstrated in figures 4-6 where the evolution of the energy spectrum of various computations are

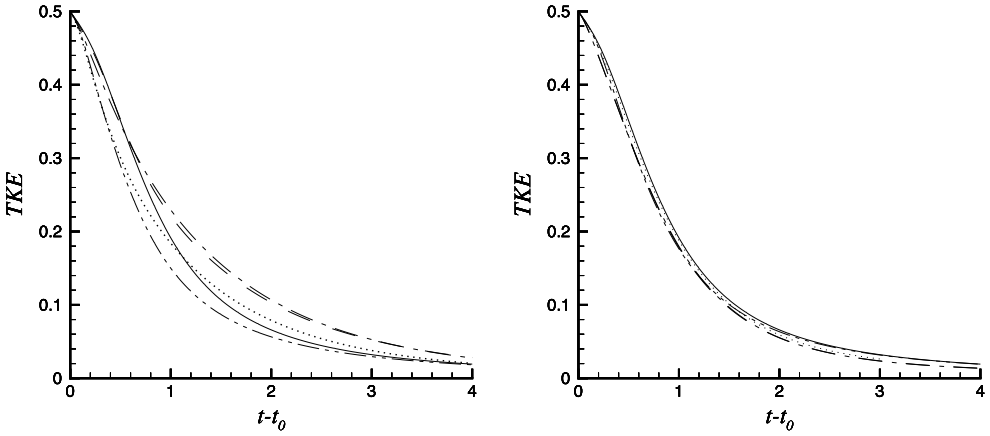

(a) (b)

FIGURE 3. Decay of kinetic energy, full DNS 128^3 (solid); (a) $N_\alpha^3 = 48^3$, LANS with $\alpha = \frac{1}{16}$ (dash dot); LANS with $\alpha = \frac{1}{8}$ (dash); dynamic LES with a filter ratio 2 (dotted); DNS sharply filtered to 48^3 (dash dot dot); (b) $N_\alpha^3 = 64^3$, LANS with $\alpha = \frac{1}{16}$ (dash); LANS with $\alpha = \frac{1}{20}$ (dash dot); dynamic LES with a filter ratio 4 (dotted); DNS sharply filtered to 64^3 (dash dot dot).

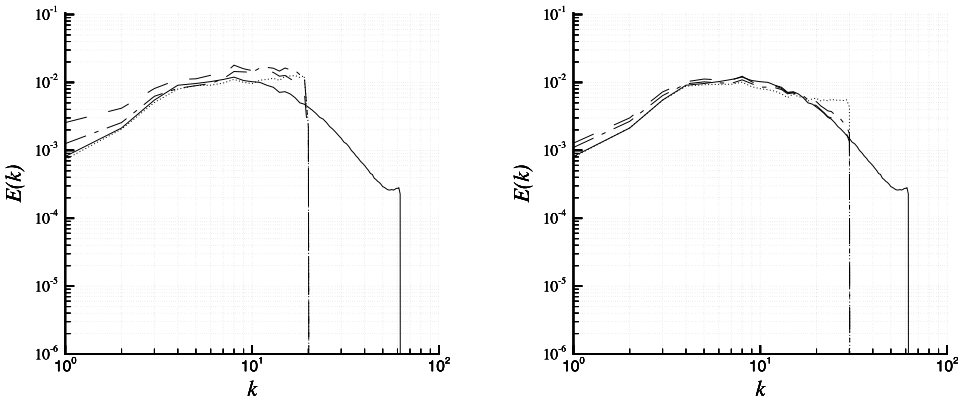

(a) (b)

FIGURE 4. The energy spectra at $t = 1$, full DNS 128^3 (solid); (a) $N_\alpha^3 = 48^3$, LANS with $\alpha = \frac{1}{16}$ (dash dot); LANS with $\alpha = \frac{1}{8}$ (dash); dynamic LES with filter ratio 2 (dotted); (b) $N_\alpha^3 = 64^3$, LANS with $\alpha = \frac{1}{16}$ (dash); LANS with $\alpha = \frac{1}{20}$ (dash dot); dynamic LES with filter ratio 4 (dotted).

presented. The pile-up of energy at higher wave numbers in the 48^3 runs indicates insufficient dissipation of energy due to inadequate resolution. This is more pronounced in the LANS computations where the model is heavily dependent on the nonlinear dispersive mechanism of the Lagrangian-averaged equations as opposed to the dissipative model in LES. For 64^3 calculations the energy spectrum is predicted reasonably well by both LANS and dynamic LES. LANS computations show better agreement for higher wave

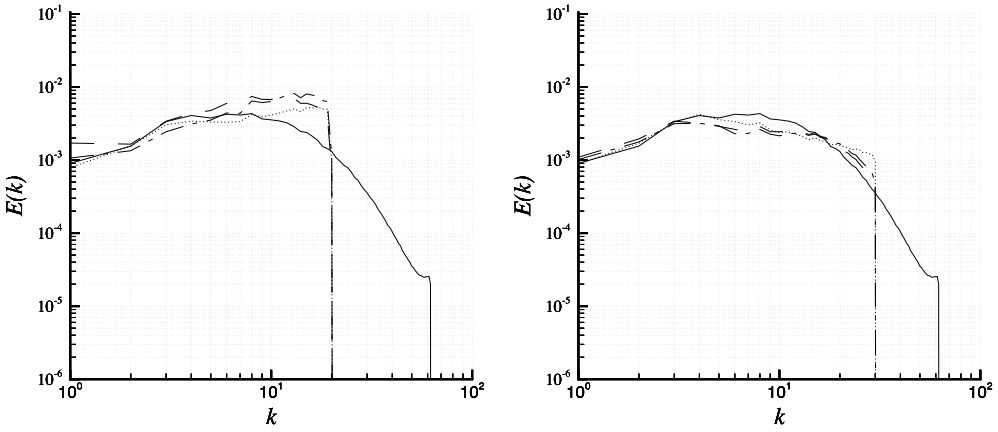

FIGURE 5. The energy spectra at $t = 2$. See figure 4 for caption.

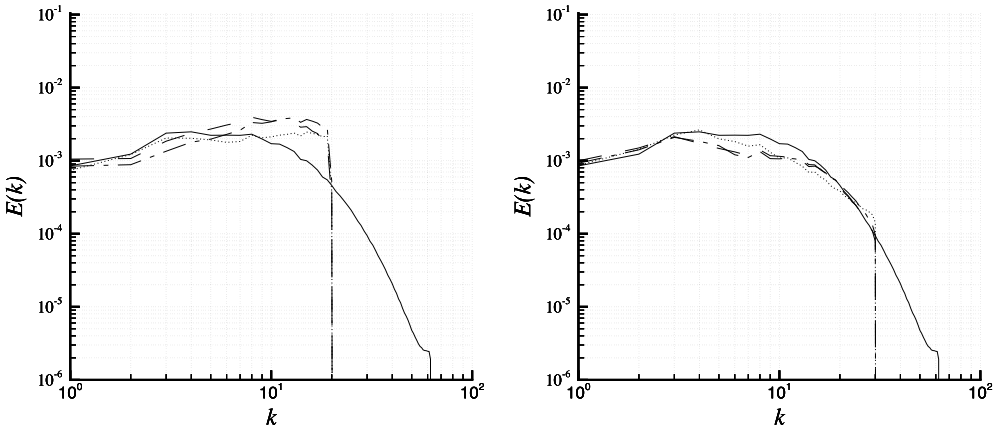

FIGURE 6. The energy spectra at $t = 3$. See figure 4 for caption.

numbers. At later times a dip at the peak of the energy spectrum is observed, which is more pronounced in LANS simulations. This might be due to the introduction of the dispersive effects in the LANS equations at scales of the order of α. However, due to the broad-band nature of the energy spectrum with the maximum of the spectrum at a relatively high wavenumber, we could not move α far from the energy-containing range. It is expected that in a higher Reynolds number flow, where there is an extended inertial range and therefore a larger gap between energy-containing scales and α scale, this effect will be diminished. Existence of such a clearance between α scales and the location of the energy peak requires resolving at least a portion of the subinertial range. LES methods will of course also work better in such a situation.

5. Conclusions and Future Directions

We studied the Lagrangian-averaged Navier-Stokes (LANS) equations through numerical simulations of isotropic decaying turbulence. Our conclusions here are made based on the numerical simulations of CBC experiments. The initial energy spectrum at $\mathrm{Re}_\lambda = 72$ is broad and the peak of the energy spectrum is around the eighth Fourier mode. Correct prediction of the TKE decay rate and the corresponding spectra for such a broad-band initial spectrum represent a difficult test case for any turbulence model.

We have demonstrated the dispersive (not dissipative) nature of the energy decay in the Lagrangian-averaged Euler (LAE) equations. This is the essence of the Lagrangian averaging method, where the energy is removed from the small scales while maintaining the crucial features of the large scale flow using dispersive rather than dissipative mechanisms. The final $E_{L_2}(\mathbf{u})$ level depends on the spectrum of the initial field, the size of the computational box, and α.

We found that, if a minimum resolution requirement (for the CBC experiments half of the DNS resolution) is satisfied, then the LANS equations provide a satisfactory turbulence closure comparable with dynamic LES. The only free parameter in LANS simulations is a length scale α which is representative of the spatial scale of the Lagrangian averaging. However, for lower resolutions both LANS and dynamic LES show a pile-up of energy at higher wave numbers. This indicates insufficient dissipation of energy due to the lack of resolution. We should point out that in LANS simulations of forced homogeneous turbulence Chen *et al.*(1999) observed a milder resolution requirement. The harsher resolution requirement in our case might be due to the broad-band nature of the initial field for the CBC experiment.

Any conclusion on the performance of the LANS equations depends on the way that the DNS data is compared with the results of LANS calculations. First of all, appropriate interpretation of the Lagrangian averaging process of the DNS data is crucial for obtaining the initial velocity field for LANS computations. The same issue arises in comparing LANS results with DNS data at later times. We considered a few different approaches. Apart from truncation of the DNS data to the resolution of LANS simulations, we have initialized LANS simulations by Helmholtz filtering or spatially averaging of the DNS data. For the CBC experiment we found that using the filter based on the Helmholtz operator or spatial averaging (top hat filter) resulted in a severe reduction of the initial resolved kinetic energy to a fraction of that of a field truncated in Fourier space (i.e., using a Fourier cut-off filter). We point out that such a reduction is independent of the model used and diminishes the value of the tests. We therefore use a sharply truncated DNS data as the initial velocity field (u) in LANS simulations.

Recently, Chen *et al.*(1999) simulated a forced homogeneous turbulent flow and reported favorable results using LANS equations. Here, we demonstrated the modeling capabilities of LANS equations in decaying turbulent flows. Apart from these satisfactory results LANS equations have many attractive theoretical features that make them a promising candidate for more complicated problems. In this process the next natural step is to test LANS models in anisotropic flows. Numerical simulation of channel flow based on the anisotropic LANS equations is the topic of our future research.

REFERENCES

Chorin, A. 1973 Numerical study of slightly viscous flow, *J. Fluid Mech.*, **57**, 785–796.

Comte-Bellot, G. and Corrsin, S. 1966 The use of a contraction to improve the isotropy of grid-generated turbulence *J. Fluid Mech.*, **25**, 657-682.

Comte-Bellot, G. and Corrsin, S. 1971 Simple Eulerian time correlation of full and narrow-band velocity signals in grid-generated isotropic turbulence *J. Fluid Mech.* , **48**, 273-337.

Germano, M., U. Piomelli, P. Moin, and W.H. Cabot 1994 A dynamic subgrid scale eddy viscosity model *Phys. Fluids A*, **3**, 1760-1765.

Foias, C., Holm, D.D., & Titi, E.S. 1999, manuscript.

Holm, D.D., Marsden, J.E., & Ratiu, T.S. 1998 Euler-Poincaré and semidirect products with applications to continuum theories *Adv. in Math.*, **137**, 1-81.

Chen, S. Y. and Foias, C. and Holm, D. D. and Olson, E. and Titi, E. S. and Wynne, S 1999 The Camassa-Holm equations and turbulence *Physica D*, **133**, 49-65.

Marsden, J.E., Ratiu, T., and Shkoller, S. 2000 The geometry and analysis of the averaged Euler equations and a new diffeomorphism group, *Geom. Funct. Anal.*, **10**.

Marsden, J. E. and Shkoller, S. 2000 The anisotropic averaged Euler equations *Archives for Rational Mechanics and Analysis*, submitted.

Oliver, M. and Shkoller, S. 2000 The vortex blob method as a second-grade non-Newtonian fluid, *Commun. PDE*, to appear.

Peskin, C.S. 1985 A random-walk interpretation of the incompressible Navier-Stokes equations *Comm. Pure Appl. Math.*, **38**, 845-852.

Rogallo, R. S. 1981 Numerical experiments in homogeneous turbulence *NASA Tech. Memo 81315*.

Shkoller, S. 1998 Geometry and curvature of diffeomorphism groups with H^1 metric and mean hydrodynamics, *J. Funct. Anal.*, **160**, 337–365.

Shkoller, S. 2000 On averaged incompressible hydrodynamics, *J. Diff. Geom.*, submitted.

Shkoller, S. 2000 Smooth global Lagrangian flow for the 2D Euler and second-grade fluid equations, *Appl. Math. Lett.*, **14**.

Wray, A.A. 1998 In A selection of test cases for the validation of large-eddy simulations of turbulent flows, *AGARD Advisory Report 345*.